International Journal of Biological Macromolecules 314 (2025) 144384

Contents lists available at ScienceDirect

International Journal of Biological Macromolecules

journal homepage: www.elsevier.com/locate/ijbiomac

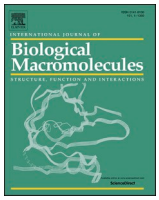

Natural sporopollenin microcarriers: Morphological insights into their functional performance for drug encapsulation and release

Volkan Aylanc [a,b,c], Andreia F. Peixoto [b], Lalehan Akyuz [d], Nuno Vale [c,e], Cristina Freire [b], Miguel Vilas-Boas [a,*]

[a] CIMO, LA SusTEC, Instituto Politécnico de Bragança, Campus de Santa Apolónia, 5300-253 Bragança, Portugal
[b] LAQV-REQUIMTE-, Departamento de Química e Bioquímica, Faculdade de Ciências, Universidade do Porto, 4169-007 Porto, Portugal
[c] PerMed Research Group, Center for Health Technology and Services Research (CINTESIS), Rua Doutor Plácido da Costa, 4200-450 Porto, Portugal
[d] Department of Molecular Biology and Genetics, Aksaray University, 68100 Aksaray, Turkey
[e] CINTESIS@RISE, Faculty of Medicine, University of Porto, Alameda Professor Hernâni Monteiro, 4200-319 Porto, Portugal

ARTICLE INFO

Keywords:
Bee pollen pellet
Green carriers
Sustained drug loading/release

ABSTRACT

Natural sporopollenin microcapsules (SMCs) derived from pollen offer versatility and efficiency for different applications, from environmental remediation to food and therapeutics delivery. A critical gap remains in understanding the relationship between SMCs morphologies and their effectiveness in drug loading and delivery. Herein, we encapsulated 5-Fluorouracil (5-FU), a model anticancer drug, into SMCs derived from seven bee monofloral pollens, each exhibiting distinct morphological features, and examined how their loading and release performance correlated with their morphology. Microscopic and particle size analyses revealed that the chemically purified SMCs were hollow, with sizes ranging from 11.0 to 35.6 μm, without significant size changes after drug loading. Encapsulation efficiency achieved through vacuum-assisted loading (18–28 %) generally surpassed that of passive and compression loading techniques. Moreover, there was a trend of increasing encapsulation efficiency with larger SMC sizes, albeit with some exceptions. In a sequential release environment simulating the in vitro gastrointestinal tract and colonic fermentation, smaller SMCs exhibited a faster release profile, whereas larger ones demonstrated a slower sustained release. The quantity and shape of apertures on SMCs walls significantly impacted their drug-loading capacity and release characteristics. Additionally, natural SMCs remained structurally intact even in the presence of digestive enzymes, varying pH levels, and colonic bacteria, indicating minimal degradation under these conditions. Overall, the findings highlight the significant influence of SMCs morphologies on their functional performance and provide a list of SMCs-based microstructures to guide drug release applications.

1. Introduction

Micro- and nanoscale building block advances, including their design, fabrication, and functionalisation, hold great promise across diverse application fields [1]. As an important member of these building blocks, microcapsules have expanded into a wide range of research areas, from environmental remediation and the stabilization of food ingredients to drug delivery systems, electronic sensors, and energy storage platforms [1,2]. Fabricated through various techniques, inorganic, organic, and hybrid microcapsules were successfully tailored to specific applications to achieve desired performance outcomes [3,4]. A trend in recent decades involves the transition to biomass as a resource for greener fabrication because biomass is advantageous due to its chemical convertibility, flexibility for modification, and abundant availability in nature [5]. Such an orientation addresses environmental concerns and underscores a commitment to fostering greener and more sustainable practices [6].

In response to the growing interest in green technologies and sustainable processes, pollen grains have emerged as a compelling option for microcapsule production. Pollen grains can be sourced directly from plants or harvested from honeybee hives, serving as renewable resources [7,8]. The technique of trapping bee pollen pellets stands out for its

* Corresponding author at: Centro de Investigação de Montanha (CIMO), Instituto Politécnico de Bragança, Campus de Santa Apolónia, 5300-253 Bragança, Portugal.
E-mail address: mvboas@ipb.pt (M. Vilas-Boas).

https://doi.org/10.1016/j.ijbiomac.2025.144384
Received 5 February 2025; Received in revised form 13 May 2025; Accepted 17 May 2025
Available online 18 May 2025

effectiveness in simplifying the collection and processing of pollen grains [2]. Furthermore, the significance of these particles is underscored by their consistently uniform size (predominantly ranging from 10 μm to 50 μm), a diverse array of geometric shapes, species-specific surface topography, apertures inherent in the pollen wall, and the presence of nanochannels [9]. These distinctive characteristics position pollen grains as versatile candidates for developing microcapsules within the context of technologically advanced applications.

In nature, pollen grains serve a vital role in protecting the genetic material and cellular components of plants against diverse environmental stressors such as harmful radiation, microbial threats, temperature extremes, and drought, thereby ensuring the maintenance of plant reproductive capabilities [10]. This protective function is primarily attributed to a sophisticated bilayer wall structure, the intine (inner layer) made of cellulose/pectin, and the exine (outer layer) composed of sporopollenin biopolymer [11]. Of particular interest to many researchers are sporopollenin microcapsules (SMCs), which yield a large internal cavity through chemical treatment (acidolysis) involving removing cellular components and the intine layer of pollen grains [12]. Apart from being resistant to diverse conditions of SMCs, the recognition of their biocompatibility and chemically or physically modifiable has opened the way for further investigation of SMCs as promising biomaterials in pharmaceutical applications, separation technology, catalytic reaction, bio-templates, water pollution remediation, and colloidal science [2,13,14]. Nevertheless, SMCs have garnered significant attention in research focused on the loading and controlled release of drugs [15,16] and bioactive substances, such as proteins [7], vaccines [17], or vitamins [18], as they serve as significant platforms for encapsulating a variety of therapeutic formulations, particularly those intended for oral administration. Given their biocompatibility, chemical resilience, and ability to maintain drug integrity in challenging environments, SMCs hold promise for real-world applications such as oral delivery of bioactive agents, sustained-release formulations, and site-specific drug targeting in gastrointestinal or colonic treatments [18].

Within the vast plant kingdom, there exists an immense diversity of pollens characterized by different morphologies [9,19]. However, the range of pollen investigated remains very limited. To expand the application of microcapsule technology for encapsulating bioactive compounds and to provide a broader range of options, we selected different types of pollen from *Castanea* sp. (Cas), *Echium* sp. (Ech), *Jasione* sp. (Jasi), *Papaver* sp. (Pap), Amaranthaceae (Ama), *Helianthemum* sp. (Hel), and *Cistus* sp. (Cis). These pollens are commonly collected by honey bees, providing an abundant raw resource while enabling their future commercial exploitation. Additionally, they exhibit diverse morphological characteristics, opening the possibility for different performances. The size, geometric shape, and apertures of sporopollenin microcapsules are known factors influencing encapsulation efficiency, interaction with biological tissues, release rate, and, ultimately, bioavailability of loaded substances [19–21]. Control over these operational parameters allows practical and theoretical evaluation of microcapsules as simple and precise drug delivery platforms. One type of microcapsule with uniform size can be selected, or several kinds of microcapsules can be mixed with desired diameters. Until now, the few studies available have predominantly examined SMCs derived from the same types of pollen like *Lycopodium clavatum* L. [15,18,22], *Helianthus annuus* L. [7,8,23], and *Pinus* sp. [19,22,24]. These works involve loading diverse drugs and bioactive substances and conducting release studies in diverse environments, thereby hindering an accurate comparison. Hence, establishing a list of SMCs tested under consistent media and conditions, complete with variable morphological characterization and functional performance data, can serve as a valuable guide for selecting the most suitable microcapsule type tailored to specific applications. Moreover, investigating the stability of SMCs under gastrointestinal and colonic conditions, and comparing them with other biopolymer-based carriers, advances the understanding and development of sporopollenin-based drug delivery systems.

Herein, we investigated seven types of pollen purified from bee pollen pellets to understand, for the first time, morpho-performance relationships and aimed to leverage them as effective drug loading and delivery systems, Fig. 1. With this aim, we compared three different encapsulation techniques (passive, vacuum, and compression loading) while loading 5-Fluorouracil (5-FU), an anticancer drug, into SMCs. Subsequently, release studies were conducted in simulated in vitro gastrointestinal tract and colonic fermentation environments. Statistical analyses, including ANOVA and *t*-tests, were performed to evaluate the significance of differences among experimental groups. Functional performances were discussed by linking SMC morphological features and the corresponding encapsulation efficiencies and release profiles.

2. Experimental section

2.1. Collection and preparation of bee pollen pellets

Bee pollen samples were harvested on hives with *Apis mellifera iberiensis* honeybees in Bragança, Portugal, between April and August 2022, using pollen traps. The mixture of bee pollen pellets was initially cleaned to remove wood residues and dead bee parts. Subsequently, under a light microscope, the pellets within the mixture were examined to identify the specific pollen types corresponding to each distinct colour. Following this identification step, the pollen pellets of interest were meticulously separated based on their shape and colours in daylight, ensuring precise colour separation. To ascertain the botanical origins of bee pollen samples, categorised by colour, a palynological analysis was conducted according to previously reported [25,26]. Samples collected on different dates were not mixed until palynological certification.

2.2. Chemical treatment of bee pollen

The purification process started with defatting, as previously outlined elsewhere [25]. Initially, 50 g of bee pollen underwent refluxing in 400 mL acetone (at 50 °C, 220 rpm, for 3 h), followed by one treatment with 400 mL water (at 50 °C, 220 rpm, for 1 h, repeated twice) and another with 400 mL acetone (at 50 °C, 220 rpm, for 3 h). After the removal of acetone, the sample was left to air dry in a fume hood for 12 h. The resulting dry sample was then stirred three times in 400 mL diethyl ether (at room temperature, 300 rpm), the first two times for 2 h and the last for 12 h. After removing the supernatant, the sample was allowed to dry in a fume hood for an additional 12 h.

In the second stage, the previously defatted pollen grains underwent acidolysis in 400 mL of 85 % (*w/v*) phosphoric acid (at 70 °C, 250 rpm) for 8 h. This was followed by a systematic washing process involving 400 mL portions: water (at 50 °C, 5 times), acetone (at 50 °C, 2 times), 2 M hydrochloric acid (at 50 °C, 1 time), 2 M sodium hydroxide (at 50 °C, 1 time), water (at 50 °C, 5 times), acetone (at 50 °C, 1 time), ethanol (at 50 °C, 2 times), and water (at 50 °C, 1 time). After each washing step, the samples were collected through a vacuum filtration system (Model DA7C, Charles Austen Pumps Ltd., Byfleet, UK). Finally, it was dried in an oven (Memmert UNE400, Schwabach, Germany) at 45 °C for 3 days before storage in a dry environment at room temperature.

2.3. Encapsulation of anticancer drug into SMCs

Different loading techniques were employed to evaluate the drug encapsulation efficiency of SMCs with varying morphological characteristics. We adapted techniques based on passive, compression, and vacuum loading, slightly modifying a method previously reported for SMCs [27].

For passive loading, approximately 50 mg 5-FU was dissolved in 1.2 mL dimethyl sulfoxide (DMSO) in a Falcon tube, followed by the addition of 100 mg SMCs. The suspension was vortexed for 10 min, and the tube was placed in a thermo shaker (ZWY-240, Labwit Scientific,

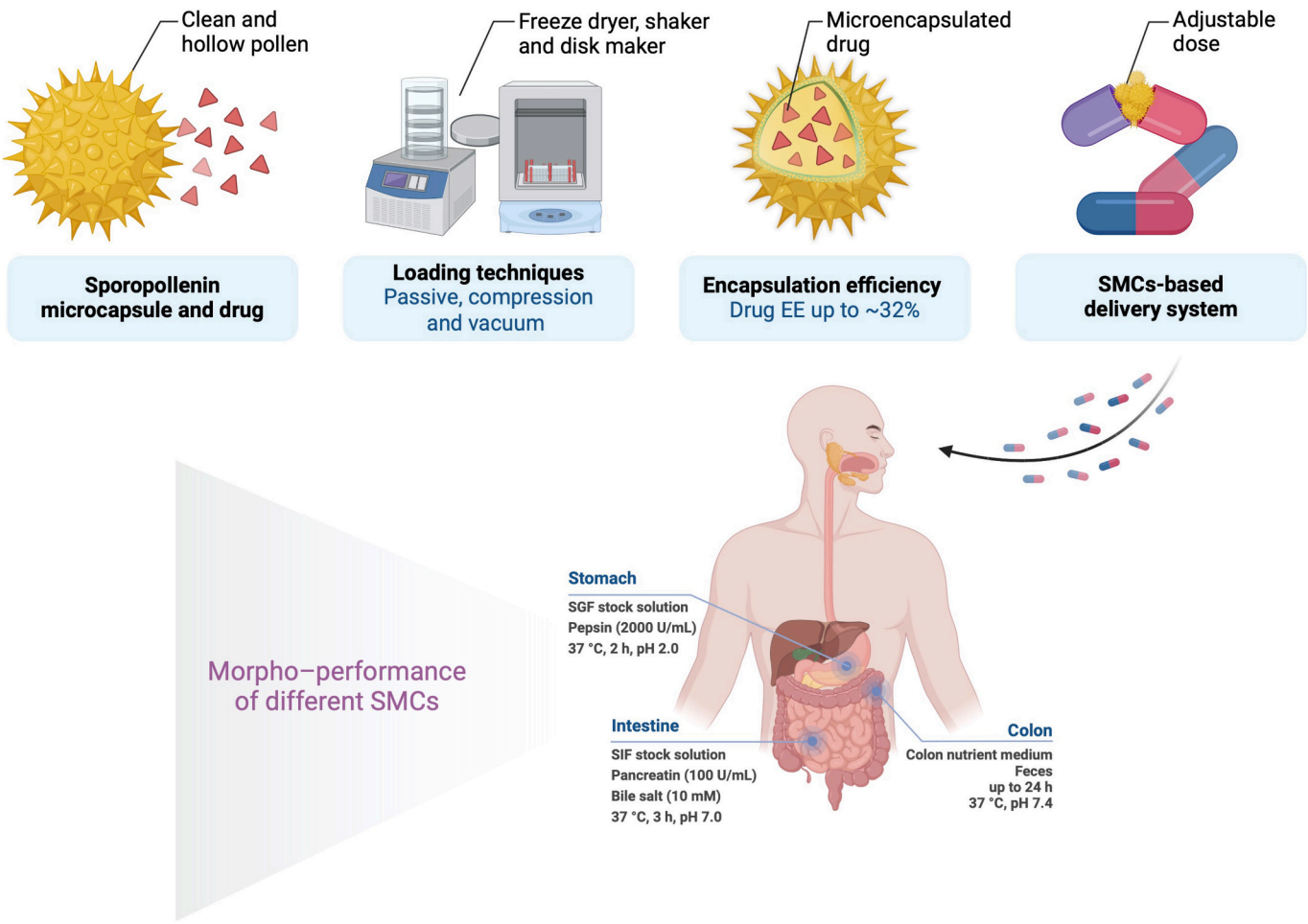

Fig. 1. Flow diagram illustrating the process of drug loading into SMCs derived from bee pollen pellets using diverse techniques, alongside their release performance in the simulated gastrointestinal tract and colonic fermentation environments.

Melbourne, Australia) set at 210 rpm, for 3 h, at room temperature. In compression loading, 100 mg of SMCs were filled in a 13 mm pellet press mould and compressed to form a tablet under a hydraulic press with a 5 t load for 20 s (mould diameter 13 mm; area 132.75 mm^2). The resulting disk was soaked in 50 mg 5-FU solution dissolved in 1.2 mL DMSO in a 25 mL flat glass bottle, for 3 h, to allow 5-FU uptake. For the vacuum loading, 100 mg of SMCs was suspended in 50 mg 5-FU solution dissolved in 1.2 mL DMSO and vortexed for 10 min. The sample was then placed in a freeze dryer (Vaco 10-II, Zirbus Technology, Bad Grund/Harz, Germany), and a vacuum of 0.5 mbar was applied for 3 h. After passive, compression, or vacuum loading, 5-FU loaded SMCs were collected by centrifugation (Multifuge X1R, Thermo Scientific, MA, USA) at 4500 rpm for 3 min. To remove 5-FU adhering to the surface of the microcapsules, they were washed using 0.5 mL of distilled water and centrifuged under the same conditions twice. Samples were frozen in the freezer at −80 °C for 30 min and then freeze-dried for 24 h. The 5-FU loaded SMCs were stored in a dry cabinet at room temperature until further usage. Placebo samples without 5-FU were prepared using the same methods for each loading technique. 5-FU loading was performed in three independent replicates for each SMC type.

2.4. Scanning electron microscopy (SEM) analysis

SEM imaging was performed with an FEI Quanta 400 FEG ESEM/EDAX Genesis X4M (FEI Inc., OR, USA) instrument at 15.00 kV acceleration voltage under various magnifications. Samples were spread on conductive carbon tapes and coated with Au/Pd using sputter coater equipment (SPI Module Sputter Coater, PA, US) (15 mA, 100 s).

2.5. Confocal laser scanning microscopy (CLSM) analysis

Confocal images were acquired using LSM 510 META with a Zeiss Axio Imager Z1 (Carl Zeiss, Oberkochen, Baden-Württemberg, Germany) and LSM 510 software (version 4.0 SP2). The same settings were applied to all images to normalise the results. The lasers used were argon (488 nm) set at 13 %, helium-neon (543 nm) set at approximately 51 %, and diode (405 nm) set at approximately 69 %. The pinhole was set to 96 mm (1.02 airy units) for the argon laser, 102 mm (0.98 airy units) for the helium-neon laser, and 112 mm for the diode laser using a 63× objective. Images were captured at a scan speed of 6 or 8 with 1 μm thick Z sections, deconvolutioned using the 3D deconvolution tool of the AutoQuant X3 software (Media Cybernetics), and processed in TIFF images with ImageJ (1.47v).

2.6. Laser diffraction particle size analysis

The particle size and particle size distribution of the SMCs and drug loaded SMCs by vacuum loading technique were measured using a Mastersizer 3000 (Malvern Panalytical Inc., Malvern, UK) based on the laser diffraction technique [28]. An average of five measurements was taken at 22 °C, with distilled water as the dispersion medium. The determined parameters were D_{10}, D_{50}, and D_{90}, representing the particle sizes corresponding to 10 %, 50 %, and 90 % of the total particle volume in the samples, respectively.

2.7. Fourier-transform infrared (FTIR) spectroscopy

FTIR measurements were carried out using the Summit X FTIR Spectrometer (Thermo Scientific Corp., MA, USA) equipped with a monolithic diamond crystal attenuated total reflection (ATR) accessory. Reflectance infrared spectra were obtained at a spectral resolution of 4 cm^{-1}, with 64 scans conducted per measurement, spanning the range from 4000 to 600 cm^{-1}. The data were processed using the OMNIC Paradigm Desktop Software (Thermo Scientific Corp., MA, USA). FTIR spectra were interpreted in their original recorded form to preserve data integrity.

2.8. Encapsulation efficiency

Approximately 10 mg of 5-FU loaded SMC were suspended in 5 mL pH 7.4 phosphate-buffered saline, vortexed for 10 min, and subjected to probe sonication (Model CY-500, Optic Ivymen System, Barcelona, Spain) at 50 % amplitude (10 cycles) for 10 s at room temperature. The mixture was centrifuged at 4500 rpm for 3 min. The supernatant was collected and passed through a 0.22 μm membrane filter with a syringe. The same procedures were performed for the placebo without 5-FU. The absorbance was measured at 266 nm using a UV/Vis spectrophotometer (Zuzi 4255/50, Auxilab, Beriáin, Navarra, Spain) with a placebo as a blank, and 5-FU released from the SMCs was quantified using a 5-FU calibration curve (1–18 μg/mL; y = 0.0512× + 0.0152; R^2 = 0.999). Encapsulation efficiency was performed in three independent replicates for each SMC type. The encapsulation efficiency of 5-FU was calculated through the following Eqs. [27]:

$$Amount\ of\ drug\ (mg) = (Absorbance \times dilution\ factor)/(Slope \times 1000)$$

$$Loading\ (\%) = (Amount\ of drug\ released / Weight\ of drug\ loaded\ SMCs) \times 100$$

$$Encapsulation\ efficiency\ (\%) = (Practical\ loading / Theoretical\ loading) \times 100$$

Theoretical loading is based on the total initial weight of the batch (150 mg).

2.9. Drug release dynamics in simulated gastrointestinal tract and colonic fermentation environments

The releasing dynamics of the drug-loaded SMCs were investigated through sequential immersion in simulated gastric fluid (SGF, pH 2.0), simulated small intestine fluid (SIF, pH 7.0), and simulated colonic fluid (SCF, pH 7.4) to mimic the environmental changes in the gastrointestinal tract and colonic fermentation following oral dosing [29,30]. 10 mg of drug-loaded SMCs were enclosed in dialysis bags with a molecular weight cut-off of 14,000 Da, containing 5 mL of SGF. Subsequently, the bags were transferred to 50 mL of SGF medium and incubated in a thermo orbital shaker (100 rpm) for 2 h at 37 °C. Following this step, the dialysis bags were transferred to 50 mL of SIF for 3 h and placed in 50 mL of SCF for up to 24 h. At predetermined time points, 2 mL of simulated digestive or colonic fluid was withdrawn from the release medium, and an equivalent volume of fresh release medium was added. After passing the released sample through a 0.22 μm membrane filter, the absorbance was measured at 266 nm against the placebo as a blank. For a detailed description of the reagents, enzymes, and the collection of faecal samples utilised in preparing the in vitro simulated gastrointestinal fluids (Table S1) and colonic fermentation media, refer to the Supplementary Information. All 5-FU release analyses were performed in three independent replicates for each SMC type.

The quantity of 5-FU released from the SMCs was determined using a UV–Vis spectrophotometer at 266 nm. The absorbance of the released 5-FU in media was plotted against the blank. The cumulative percentage of released 5-FU was calculated using the following Eqs. [31]:

$$Concentration\ of\ drug\ (mg/mL) = (Absorbance \times Slope) \pm \text{intercept}$$

$$Amount\ of\ 5-FU\ (mg) = (Concentration \times Dissolution\ bath\ volume)$$

$$Cumulative\ release\ (\%) = (Volume\ of\ sample\ withdrawn\ (mL) / Bath\ volume\ (mL)) \times P(t-1) + Pt$$

Pt is the rate of free release at time t, and P (t - 1) is the rate of free release before t.

2.10. 5-FU release kinetics studies

The drug release pattern on encapsulated devices can be understood using different models, allowing the design of an effective formulation, but also validating the release mechanism through experimental data. In this work, we explored four kinetic models, such as zero order, first order, Higuchi, and Korsmeyer-Peppas [32]. These kinetic models were selected due to their broad applicability in characterizing drug release from micro- and nano-structured carriers. Their approach represents key release mechanisms, such as constant release, concentration-dependent release, and diffusion through porous matrices, making them particularly suitable for evaluating the performance of SMCs. Model fitting was performed using Excel (Microsoft Corporation, Washington, USA), and the coefficient of determination (R^2) was used to assess the fit adequacy for each kinetic model.

Zero-order release kinetics model refers to the process of time-dependent drug release from a drug delivery device, independent of the concentration. The zero-order release can be represented as:

$$Q_t = Q_0 + k_0 t$$

where Q_t represents the amount of drug released or dissolved in time t, Q_0 is the initial amount of drug release (generally $Q_0 = 0$), k_0 is the zero-order release constant, and t is the time. The cumulative amount of drug released can be plotted against the time.

For first-order release kinetics, the changes in concentration during time evolution are dependent only on the concentration available, expressed by the equation:

$$logQ_t = logQ_0 + k_1 t/2.303$$

where Q_t is the amount of drug released on time t, Q_0 is the initial amount of drug in solution, k_1 is the first-order release constant, and t is time. An example of this behaviour can be found in active substances incorporated in porous delivery devices, where the remaining drug in the device is proportional to the released drug, decreasing over time. For this situation, the log cumulative of % drug remaining can be plotted against the time.

The Higuchi model describes drug release kinetics from a porous matrix system where the drug solubility in the medium is lower than the drug loaded in the delivery device and is expressed by the simplified square root of the time equation:

$$Q_t = Q_0 + k_H t^{1/2}$$

Where Q_t and Q_0 have the same meaning as above, k_H is the Higuchi constant and t is the time. It is also important to note that the Higuchi constant accounts for different parameters of the matrix, such as the porosity. For this situation, the cumulative amount of the released drug can be plotted against the square root of time.

The Korsmeyer and Peppas model describes both Fickian and non-Fickian drug release from swelling and non-swelling polymeric carrier systems:

$$M_t/M_\infty = kt^n$$

where M_t denotes the mass of the drug released over time t, M_∞ is the amount of drug at the equilibrium state (sometimes very close to the

amount of drug contained in the dosage form at the beginning of the release process), k is a constant which incorporates structural information of the delivery system and the drug, and n is the exponent of release (related to the drug release mechanism) in the function of time t.

2.11. Statistical analysis

Statistical analysis was conducted using GraphPad Prism 9.5.1 (San Diego, CA, USA). A two-tailed *t*-test was employed for comparisons involving two variables, while ANOVA with post hoc Tukey test was applied for comparisons involving more than two variables. This approach effectively controls the type I error rate while allowing for multiple comparisons. Additionally, the post hoc Tukey test is appropriate for datasets with approximately equal sample sizes and variances, which align with the characteristics of our experimental data. Encapsulation and release experiments were conducted with a minimum of three independent replicates, and all data are presented as mean ± SD. Significance levels of the *p*-value are denoted as follows: 0.01 to 0.05 (*), 0.001 to 0.01 (**), and < 0.001 (***).

3. Results and discussion

3.1. Morphological characterization of SMCs

Seven distinct types of pollen, namely Cas, Ech, Jasi, Pap, Ama, Hel, and Cis, were selected to investigate the morpho-performance of SMCs. This exploration focused on three different techniques for drug loading and the release behaviour within an in vitro simulated gastrointestinal tract and colonic fermentation. The samples were considered from plants commonly visited, whose pollen is collected by honeybees, and were noteworthy for their diverse morphologies.

A three-step chemical method was employed to fabricate SMCs from bee pollen pellets. In the initial defatting step, the oily layer, known as the pollenkitt [33], covering the surface of the pollen grains was eliminated using acetone, water, and diethyl ether. Subsequently, phosphoric acid (85 % (*w/v*) refluxing was performed to eliminate cellular materials other than exine. The concluding washing step involved water, organic solvents, and acidic and alkaline solutions to eliminate residual pollen components and yield clean SMCs. SEM analysis confirmed the effectiveness of the applied method, yielding intact pollen microcapsules, as shown in Fig. 2a and Fig. 3a. The SEM images also revealed the opening of apertures along the pollen wall, particularly in areas where the exine is thin or absent—typically coinciding with the location of the intine layer [34]. This phenomenon may facilitate the loading of bioactive substances into the microcapsules.

A crucial consideration is ensuring the complete removal of pollen interiors before encapsulating drugs or other substances in SMCs, providing a spacious internal cavity. Notably, the biomolecules within the inner cavity of pollen grains, along with sporopollenin itself, exhibit autofluorescence across a broad wavelength spectrum [12]. Taking advantage of this characteristic, we conducted CLSM analysis and observed autofluorescence in the inner cavity of raw pollen, Fig. 2b. In contrast, the treated SMCs exhibited no autofluorescence, clearly demonstrating the successful removal of cellular material and achieving hollow SMCs, Fig. 3b. The effectiveness of removal could also be checked using SEM from manually crushed raw pollen grains and SMCs from the Jasi type, demonstrating the effectiveness of the chemical method in achieving a clean inner cavity, Fig. S1.

Each plant species generally produces distinct types of pollen characterized by differences in size, shape, the number of apertures on the pollen surface, and surface ornamentation, Table 1. Among the types studied, including Jasi, Pap, Ama, Hel, and Cis, a predominantly spherical structure was observed, with an aspect ratio close to one, while Cas pollen grains were classified as flattened, and Ech pollen grains were categorised as prolate-heteropolar [25,26]. All pollen types exhibited a tricolporate aperture positioned on the surface, except for Ama (> 6). However, in the case of Pap, the surface aperture shape differed from the others, extending along the colpus. Jasi, Pap, and Ama displayed a microechinate surface ornamentation, while Hel had perforate-striate. Cas, Ech, and Cis showed rugulate, perforate, and reticulate surface ornamentation, respectively.

The size of SMCs is an important parameter for loading and release studies and was determined by laser diffraction particle size analysis. The mean diameters of the purified SMCs were 10.4 ± 0.1 μm (Cas), 16.9 ± 0.1 μm (Ech), 17.3 ± 0.0 μm (Jasi), 18.0 ± 0.0 μm (Pap), 22.6 ± 0.1 μm (Ama), 24.0 ± 0.0 μm (Hel), and 35.8 ± 0.0 μm (Cis), Fig. 4, confirming a diversity between the pollens under study, and consequently on the loading capacities.

3.2. Chemical characterization of SMCs

To further analyse the samples under study, we utilised FTIR-ATR spectroscopy, which offers insights into their chemical structure by identifying the various functional groups present [35]. Functional group assignments in the spectra were made with reference to previous studies [16,19,34,36]. The FTIR spectra of SMCs produced from bee pollen pellets were similar to each other, as shown in Fig. 5a. A broad vibration around 3300 cm^{-1} was attributed to O—H stretching in carboxylic acids, alcohols, carbohydrates, or water. The peaks at 2924 cm^{-1} and 2852 cm^{-1} corresponded to the asymmetric and symmetric C—H stretching vibrations of methylene groups (CH_2). The peaks at 1660 cm^{-1} and 1511 cm^{-1} were associated with the asymmetric stretching of non-conjugated C═C bonds, likely due to aromatic and phenolic compounds in sporopollenin biopolymer. Meanwhile, the vibration at 1570 cm^{-1} was assigned to the asymmetric stretching of carboxylate anions (COO^-). The peak at 1436 cm^{-1} was attributed to C—H stretching in the aromatic ring of sporopollenin. The vibration at 1280 cm^{-1} was assigned to C—O stretching in alkyl esters, with its intensity being more pronounced in Cas, Ama, and Hel type SMCs than in others. Finally, the vibrations at 1096 cm^{-1} and 990 cm^{-1} corresponded to the pyranose ring of sugars, representing skeletal vibrations of C–OH and C–O–C.

The FTIR spectra of 5-FU, placebo SMCs, and drug-loaded SMCs are shown in Fig. 5b–5h. The characteristic bands observed in the 5-FU spectrum, spanning 3170 cm^{-1}–2780 cm^{-1}, are attributed to the stretching of N—H bonds [37]. The peak assigned to O—H stretching around 3340 cm^{-1} in SMCs shifted to 3370 cm^{-1} in placebo SMCs [35]. Nonetheless, NH stretching bands of the 5-FU guest molecule could still be discerned in the spectra of loaded SMCs, even though overlapping with a strong and broad band originating from hydrogen-bonded OH groups. The peaks observed at 2924 cm^{-1} and 2852 cm^{-1} in SMCs and assigned to asymmetric and symmetric C—H stretching vibrations remained unchanged in placebo SMCs samples [35], and their intensity did not change significantly after the drug loading. The peak at 1720 cm^{-1} in pure 5-FU drug, which appeared as a shoulder, is assigned to C═O stretching and was also discernible in the spectra of some drug-loaded SMCs. The strong vibration at 1652 cm^{-1} in the pure drug is attributed to C═O and C═C stretching, whereas the 1660 cm^{-1} peak in the placebo SMCs spectra was assigned to asymmetric stretching of unconjugated C═C due to aromatic and phenolic compounds in the sporopollenin, as in SMCs [35,38]. For drug-loaded SMCs, this peak remained at 1660 cm^{-1} but exhibited more intense vibration. The peak recorded at 1652 cm^{-1} for 5-FU is observed to shift towards 1660 cm^{-1} due to electrostatic interactions between the drug and SMC surface. This situation is more evident when the increase in drug loading capacity is higher, especially in compression and vacuum loading techniques. This observation suggests that 5-FU did not undergo any chemical modification during its loading into SMCs, corroborating existing literature data [37]. Moreover, the sharp vibrations at 1424 cm^{-1} and 1244 cm^{-1} in the 5-FU spectrum, were attributed to C—N and C—F stretching, respectively [37]. When the C—F peak at 1244 cm^{-1} was analysed, the peak was more evident and its intensity increased, as the 5-FU loading capacity of SMCs increased. The intensity of these vibrations was

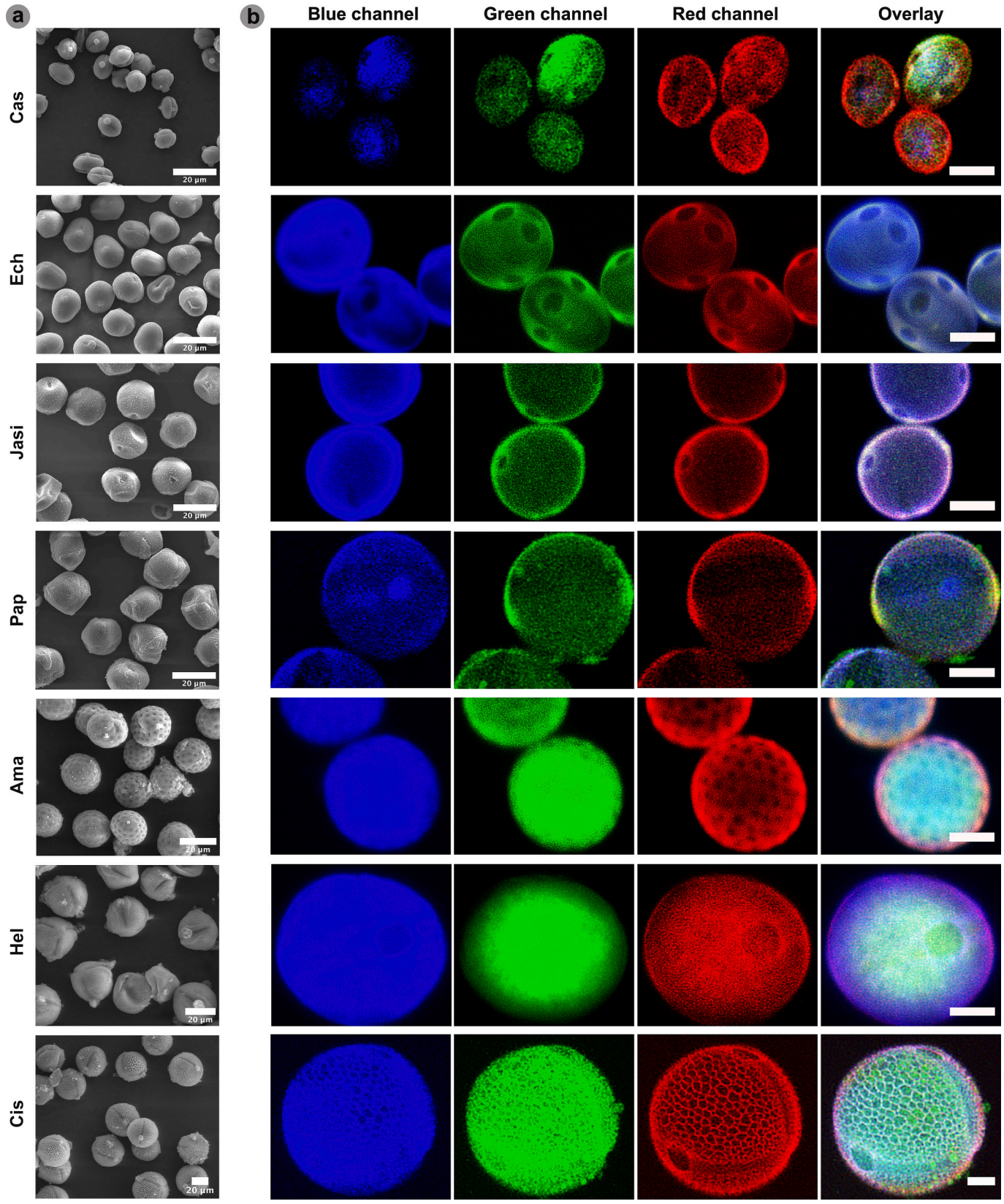

Fig. 2. Microscopic characterization of raw bee pollen grains from different botanical origins. SEM images of raw pollen grains (a), and CLSM images of raw pollen grains (b). CLSM scale bars are 10 µm.

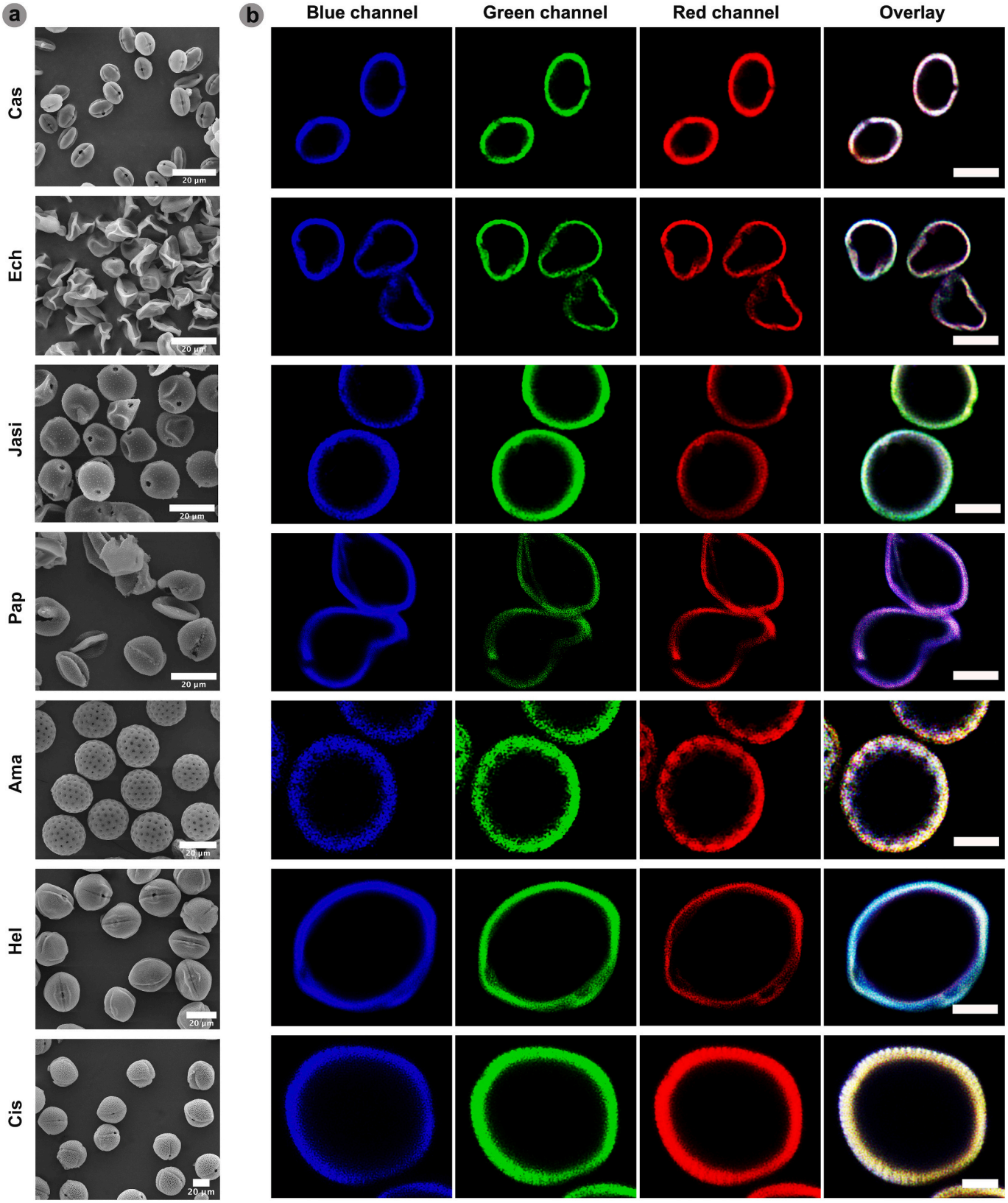

Fig. 3. Microscopic characterization of SMCs produced by chemical treatment of raw bee pollen. SEM images of SMCs (a), and CLSM images of SMCs (b). CLSM scale bars are 10 µm.

Table 1
Morphological features for the different types of SMCs within the study.

SMC type	Shape	Surface ornamentation	Shape and number of apertures	Diameter of apertures (μm)
Cas	Ellipse	Rugulate	Tricolporate; 3	1.4 ± 0.2
Ech	Prolate, heteropolar	Perforate	Tricolporate; 3	0.5 ± 0.0
Jasi	Spheroidal	Perforate, microechinate	Triporate; 3	1.8 ± 0.1
Pap	Spheroidal	Perforate, microechinate	Tricolpate; 3	Along the colpus
Ama	Spheroidal	Perforate, microechinate	Pantoporate; > 6	1.4 ± 0.0
Hel	Spheroidal	Perforate, striate	Tricolporate; 3	3.1 ± 0.1
Cis	Spheroidal	Reticulate	Tricolporate; 3	3.1 ± 0.1

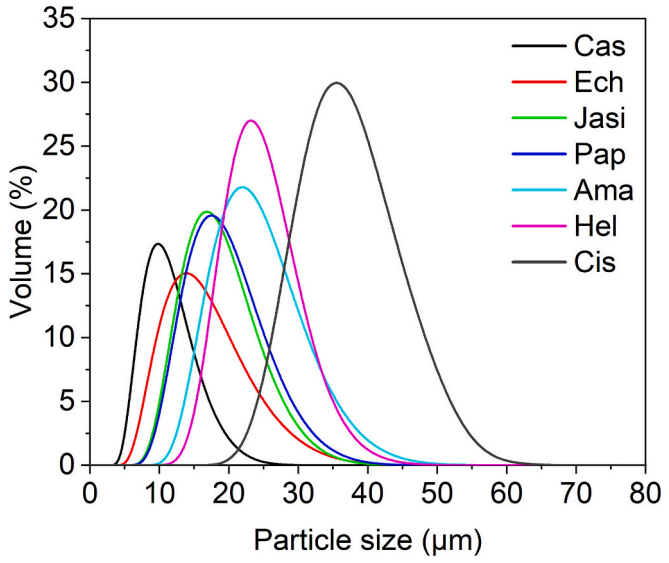

Fig. 4. Laser diffraction particle size analysis of SMCs purified from various types of pollen.

notably amplified in drug-loaded SMCs compared to placebo SMCs.

Overall, characteristic peaks attributed to 5-FU in the loaded SMCs, as illustrated in Fig. 5, confirm successful drug encapsulation. All of the abovementioned features are clear, highlighting specific regions on FTIR spectra for 5-FU loaded Cis SMCs, Fig. 5i-5k. These findings are consistent with previous FTIR spectroscopy results reported for 5-FU loaded polymer-based microcapsules and nanofibers, including polycaprolactone, chitosan, and cellulose [39–41].

3.3. Morpho–performance relationships of SMCs on drug encapsulation and release

For loading 5-FU into empty SMCs, 50 mg of the drug was fully dissolved in 1.2 mL DMSO. The high solubility of the drug in this solvent facilitates a greater loading capacity into SMCs, which might otherwise be restricted due to the limited aqueous solubility of the drug. Upon suspending SMCs in the 5-FU solution, the drug could permeate their internal cavities through apertures in the SMCs and nanoscale channels along the wall [42–46]. To optimise the loading process, three different loading techniques were evaluated with a weight ratio of SMCs to 5-FU at 2:1, which yielded optimal encapsulation efficiency based on reported data [16,27].

The encapsulation efficiencies achieved for the various SMC types are presented in Fig. 6a. Across the seven different SMCs, the efficiencies of passive, compression, and vacuum techniques ranged from 12 ± 1 (Cas) to 23 ± 1 (Cis), 14 ± 1 (Cas) to 33 ± 1 (Cis), and 18 ± 1 (Cas) to 28 ± 1 (Hel), respectively. Among these techniques, passive loading yielded the lowest efficiencies for all but Pap SMCs. On the other hand, vacuum loading resulted in the highest encapsulation efficiencies, except for Ama and Cis type SMCs. The low encapsulation efficiency of passive loading can be attributed to air pockets in the microcapsules, which arise from the surface tension between the air pockets within the SMCs and the 5-FU solution [7]. In contrast, the vacuum loading technique demonstrated notably higher encapsulation efficiency than the compression and passive methods. It is also worth mentioning that the structural integrity of the SMCs remained intact even after compression at a pressure of 5 t for 20 s, owing to the elastic feature of the sporopollenin biopolymer [12], Fig. 6b–6c. These characteristics contributed to the high efficiency of vacuum-assisted loading, potentially due to the creation of a negative pressure differential during the evacuation of air from the internal cavity of the SMCs via vacuum. Similar results were reported by Potroz et al. [7], where the vortex step improved encapsulation efficiency compared to passive loading in microcapsules derived from sunflower (*Helianthus annuus* L.); nevertheless, vacuum assistance was required to further increase the loading capacity of bovine serum albumin (BSA) into sunflower microcapsules.

Another critical aspect to consider is the relationship between the loading of 5-FU into SMCs and their morphology, which may influence encapsulation efficiency. Laser diffraction particle analysis, after drug loading, showed that the particle sizes for Cas, Ech, Jasi, Pap, Ama, Hel, and Cis were 9.9 ± 0.0 μm, 15.6 ± 0.1 μm, 17.3 ± 0.0 μm, 17.0 ± 0.7 μm, 22.6 ± 0.0 μm, 23.6 ± 0.0 μm, and 34.9 ± 0.0 μm, respectively, Figs. 6d. These results indicated no significant differences compared to empty SMCs. There appears to be an increasing trend in encapsulation efficiency from Cas type SMCs, which have the smallest sizes, to those with larger sizes, culminating in the highest rate observed in Cis type SMCs. This phenomenon could be attributed to several factors: i) The smaller the size of SMCs, the shorter the distance 5-FU molecules need to diffuse to enter the internal cavity. However, this increased resistance to mass transfer may complicate the efficient diffusion of the drug into the SMCs [47]. ii) Smaller SMCs have a higher surface area-to-volume ratio than larger ones, resulting in a larger proportion of them being in direct contact with the surrounding environment. This may lead to increased loss of encapsulated 5-FU through diffusion or interaction with the environment during the washing procedure [48]. iii) Smaller microcapsules often exhibit stronger interactions between the loaded compounds and the shell material because of reduced inner volume relative to the shell. Such interactions may impede the diffusion of additional drug into the cavity of SMCs or lead to further loss of the drug due to adsorption on the shell surface [49]. However, among the samples analysed in this study, there was a decrease in the encapsulation efficiency of Pap and Ama type SMCs, which were classified as medium-sized despite the expectation of an increase in encapsulation efficiency with an increase in size. The morphology of Pap type SMCs, Fig. 6e, with long apertures classified as tricolpate, featuring three colpus-type openings starting from one polar region and continuing towards the other polar region, and Ama type SMCs, Fig. 6f, with more than six pore-type apertures, may provide evidence that their morphology could significantly impact drug loading.

As outlined in the methods section, SMCs were washed twice to remove any drug residues from their surface after loading 5-FU. The SEM analysis of samples from the vacuum-assisted loading technique revealed the absence of noticeable drug residues on their surface, Fig. 7, confirming the successful encapsulation of the drug into the internal cavity of the SMCs. While the washing step effectively removed the unloaded drug from the medium and the surface of SMCs, it may have also resulted in the encapsulated drug flowing out again through diffusion. In particular, the relatively low loading efficiencies of the Pap and Ama type SMCs could be attributed to the washing process due to their morphology. Our findings are in agreement with reported results stating that BSA-loaded pine pollen (*Pinus massoniana*) achieved a

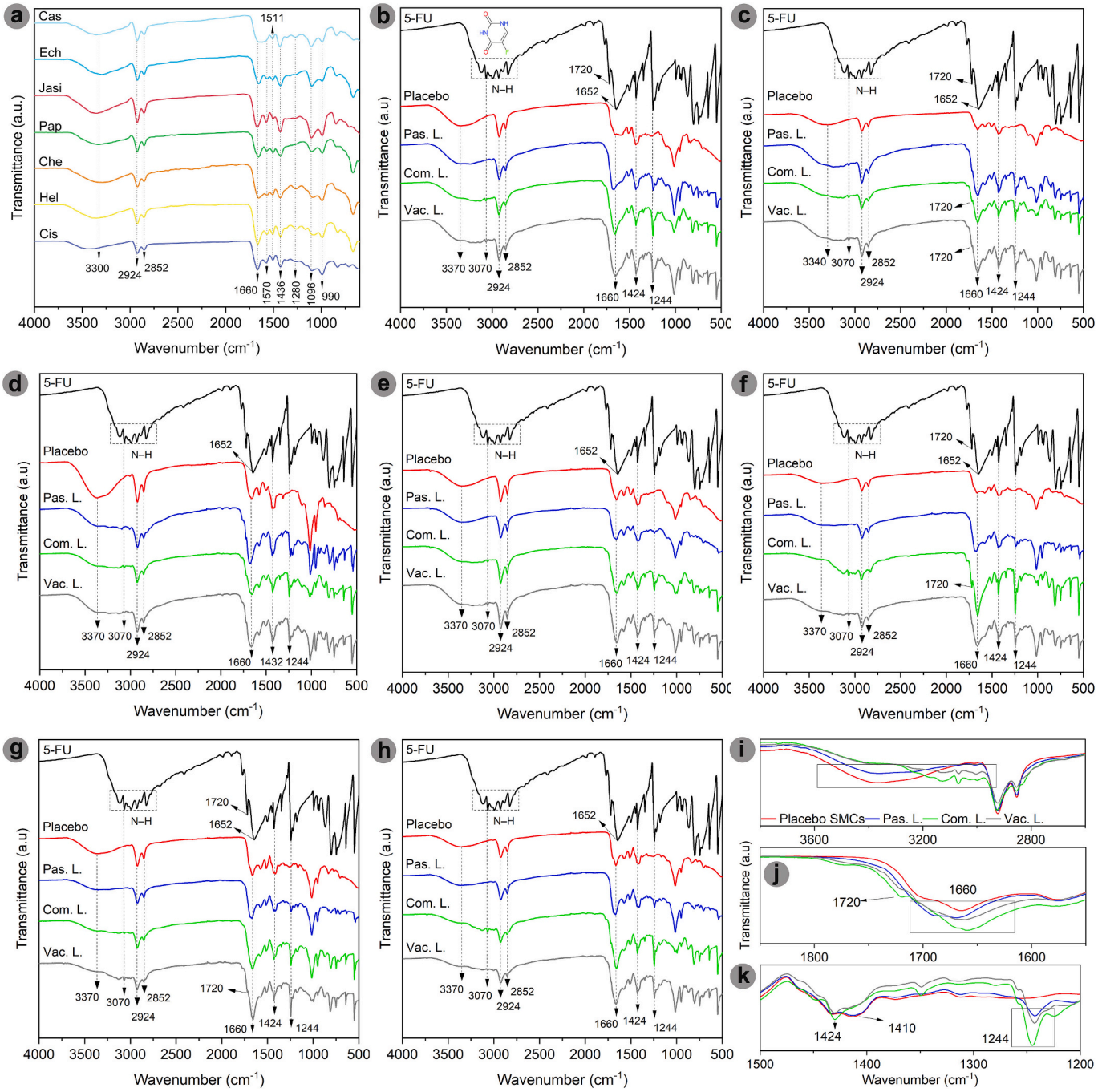

Fig. 5. FTIR spectra of SMCs obtained after the chemical treatment of bee pollen (a). FTIR spectra of pure 5-FU, placebo SMCs, and drug-loaded SMCs: (b) Cas-type, (c) Ech-type, (d) Jasi-type, (e) Pap-type, (f) Ama-type, (g) Hel-type, and (h) Cis-type SMCs. Specific FTIR regions confirming successful drug loading into SMCs (Cis-type) via passive, compression, and vacuum loading methods: (i) O—H stretching peak around ~3340 cm^{-1}, (j) C═O peak at 1720 cm^{-1}, and C═O/C═C stretching peaks at 1660–1652 cm^{-1}, and (k) C—N and C—F stretching peaks at 1424 cm^{-1} and 1244 cm^{-1}.

loading efficiency of 28 ± 2 % without washing, which decreased to 14 ± 1 % and 6 ± 2 % after the first and subsequent second washing, respectively [24]. Despite the reduction in encapsulation efficiency caused by the washing process, it is essential to note that the loaded material should occupy the inner cavity of the microcapsules rather than the outer surface. This ensures protection from external environmental factors, prevents unwanted leakage, and avoids uncontrolled release [18].

To further investigate the morpho-release performance of SMCs loaded with 5-FU, we conducted an in vitro study simulating the gastrointestinal tract and colonic fermentation environment following the route of orally taken drugs. For release analysis, SMCs loaded by the vacuum method were selected because they provided higher levels of encapsulation compared to SMCs loaded by passive and compression loading, and these levels were statistically significant ($p < 0.05$) for all four SMCs types. Fig. 8a and Fig. S2 shows the release assay results of 5-FU and seven types of SMCs sequentially in SGF at pH 2.0, SIF at pH 7.0, and SCF media at pH 7.4 for up to twenty-four hours, whereas Fig. 8b illustrates the release performance of Cis type SMCs against 5-FU in SGF media at pH 2.0 for the initial 90 min. The release of the drug molecule in SGF ranged from 54 ± 2 % (Cis) to 67 ± 8 % (Cas) within the first 30 min, depending on the type of SMCs, and reached a maximum of 82 ± 1

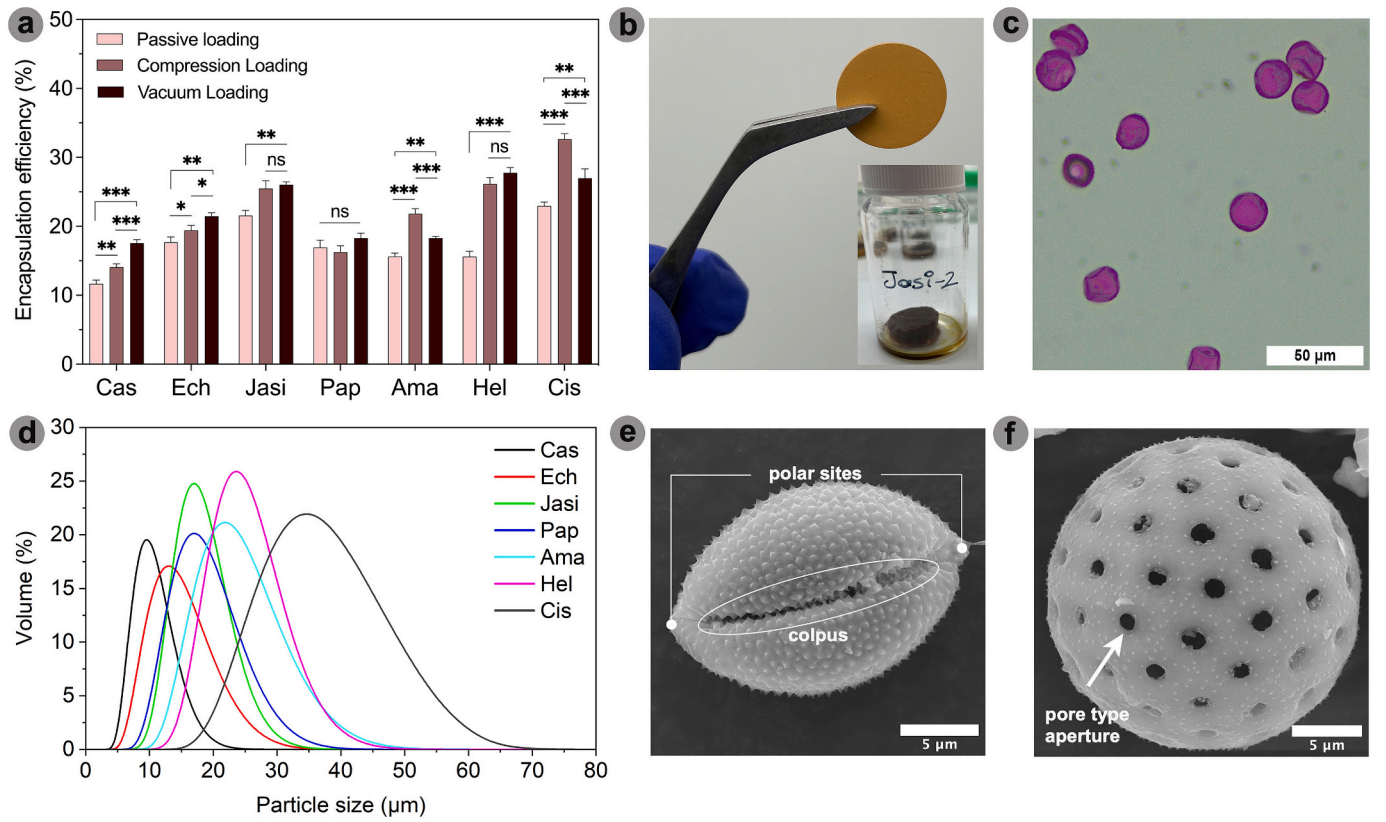

Fig. 6. Encapsulation efficiencies of 5-FU in various SMCs using passive, compression, and vacuum loading techniques (a). Jasi-type SMCs in tablet form, compressed using a hydraulic press (5 t, 20 s), shown in a swollen state after exposure to the 5-FU solution (b), followed by an optical microscope image confirming their structural integrity one hour after immersion (c). Size distribution of drug-loaded SMCs using the vacuum loading technique (d). SEM image of aperture details of Pap (e) and Ama (f) type SMCs correlating with drug loading and release. Drug loading data are presented as mean ± standard deviation ($n = 3$). Statistical significance is indicated as follows: 0.01 to 0.05 (*), 0.001 to 0.01 (**), and < 0.001 (***).

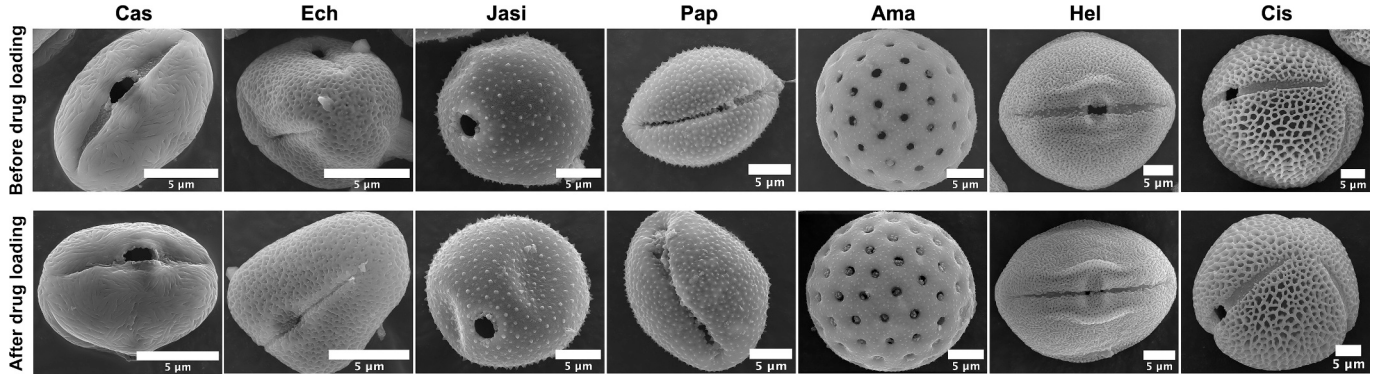

Fig. 7. SEM images of SMCs before and after drug loading using vacuum loading.

% at the end of the gastric phase (two hours) in Ama type SMCs. The observed drug-releasing dynamics in the SGF medium are attributed to the passage of molecules through micron-sized apertures along the walls of SMCs. Furthermore, there were statistically significant differences in the release rate from loaded SMCs among different types compared with 5-FU ($p < 0.05$).

In all cases, the in vitro release of 5-FU exhibited a biphasic profile, beginning with an initial burst release, followed by a relative plateau after one hour. Depending on the type of SMCs, between 59 ± 6 % (Cis) and 74 ± 2 % (Cas) of the total 5-FU was released within the first hour, followed by a sustained release phase over the next twenty-three hours. The initial burst release may be attributed to the rapid dissolution of 5-FU located near the apertures of loaded SMCs with lower interaction with the inner SMCs surface. In contrast, the subsequent controlled release phase is likely governed by the gradual diffusion of 5-FU encapsulated from within the inner cavity of the SMCs, as well as by drug molecules physically bound to the SMC inner surface through electrostatic interactions, van der Waals forces, or hydrogen bonding [50]. Additionally, the receptor medium may require time to penetrate the SMCs, dissolve the encapsulated 5-FU, and facilitate its release through surface apertures. Subsequently, among the SMCs showing release profiles in colonic conditions, up to twenty-four hours, the highest ratio was observed in the Ama sample, with a value of 88 ± 1 %, while the lowest was for Cis type SMCs, with 69 ± 4 %. The high release rate in Ama type SMCs could be attributed to the presence of multi-porous apertures on their surface. The release profiles of SMCs in SCF

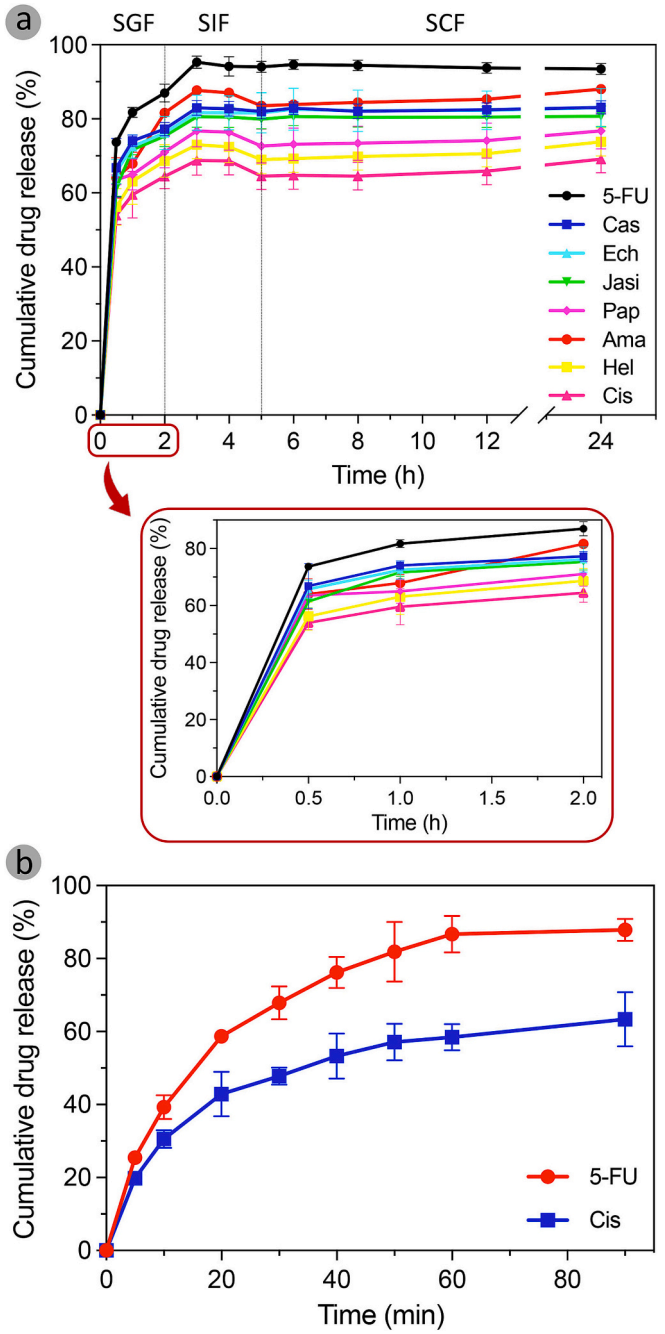

Fig. 8. Cumulative drug release profiles of seven different SMC types, over time, in simulated gastrointestinal tract and colonic fermentation media (a). Release performance of Cis-type SMCs in SGF medium (pH 2.0) during the first 90 min (b). Drug release data are presented as mean ± standard deviation (n = 3).

showed no significant ($p < 0.05$) differences compared to SIF. Another noteworthy point of the microcapsule release profile was a decrease in drug release for certain SMC types at the fourth hour in the SIF medium. This reduction observed in Pap, Ama, Hel, and Cis type SMC may be attributed to changes in the solubility of 5-FU with pH. As a drug containing both acidic and basic functional groups, 5-FU tends to dissolve more readily at lower pH levels, while its solubility may decrease under basic conditions [51]. This could explain the stabilization of release after the fourth hour. Supporting this observation, Solhjoo et al. [50] reported that 5-FU exhibits a higher binding affinity to nanocarrier surfaces at physiological pH (7.4) and demonstrates greater release under acidic conditions (pH 5.0). The release trend observed in the gastric and intestinal environment indicates rapid release, attributed to the high aqueous solubility of 5-FU. Nevertheless, the presence of apertures in all SMCs types may have further accelerated this rate. However, the release dynamics of all SMCs types suggest that they act as a barrier to delay the release of the drug for a longer duration compared to unencapsulated 5-FU, supporting previous studies on natural microcapsules from pollen grains loaded with different active substances [18,24,27].

Another critical consideration of morpho-release performance is the differential behaviour observed among natural microcapsules of varying sizes. Smaller microcapsules, such as Cas, Ech, and Jasi, exhibited faster release rates, while larger-sized Pap, Hel, and Cis type SMCs displayed a slower and more controlled release profile, except for Ama. The microcapsule size influences the rate of encapsulated drug diffusion through the microcapsule shell; larger microcapsules have a greater distance between the encapsulated drug and the SMC surface, resulting in a more extended diffusion pathway and, consequently, slower release rates [47]. Moreover, the reduced interfacial area between the SMCs and the release environment could contribute to the slower cumulative release profile of drug molecules from larger SMCs [48]. Earlier work revealed that as the size of microcapsules fabricated from starch and poly(lactide) increases, the release rate of avermectin and recombinant human insulin decreases [20]. Similar findings regarding release profiles were also reported for microcapsules derived from other types of pollen such as *Lycopodium clavatum* L. [12,52], *Phoenix dactylifera* L. [16], and *Helianthus annuus* L. [7]. Nevertheless, and considering the controlled release that we aim to achieve with SMCs, further coating with polymers such as alginate, chitosan, and cellulose seems worth investigating to achieve adjustable release performance in the desired region of the gastrointestinal tract. Such a coating can prevent an initial burst release and provide a more sustained release, which could be highly beneficial for oral dosage formulations targeting gastrointestinal diseases. Overall, our results suggest that the size of SMCs, the number of apertures, and their shape may play a role in drug encapsulation and release mechanisms.

To answer whether 5-FU-loaded SMCs had structural distortions in their micro- and nanoscale structures after exposure to the gastrointestinal tract and colonic fermentation media, we collected the samples and conducted SEM analysis. After twenty-four hours of incubation in gastric, small, and large intestinal environments, respectively, no noticeable changes were observed in their three-dimensional structure, Fig. 9. However, there were indications of some minor deformations on the surface of the exine at the nanoscale, as observed in Cas and Ech SMCs types. These findings demonstrate that various natural microcapsules could maintain their integrity for extended periods, even in the presence of enzymes and colonic bacteria, suggesting that these factors do not significantly contribute to their degradation.

To contextualize the encapsulation efficiency and release performance achieved in our systems, we compared them with values reported for other biopolymer-based carriers used in similar applications. As shown in Table 2, the efficiency of SMCs is comparable to that of several delivery systems, along with SMCs exhibited the advantage of maintaining structural integrity, especially over long periods of time. Although starch-based microcapsules showed sustained drug release reaching 82 % at pH 1.2 and 7.0, the non-uniform particle size and shape may limit their applicability [53]. Similarly, cellulose-based microcapsules showed a high encapsulation efficiency of 33 wt% with controlled release over 120 h but suffered from low thermal stability and poor three-dimensional structural integrity [54]. In contrast, SMCs derived from various pollen types in this study showed encapsulation efficiencies ranging from 12 % to 33 %, with vacuum-assisted loading generally achieving the highest efficiency. Notably, the encapsulation efficiency of SMCs was influenced by size, number of apertures and morphology, with larger microcapsules exhibiting higher loading capacities. The release profile of 5-FU-loaded SMCs followed a biphasic pattern with initial immediate release followed by continuous diffusion.

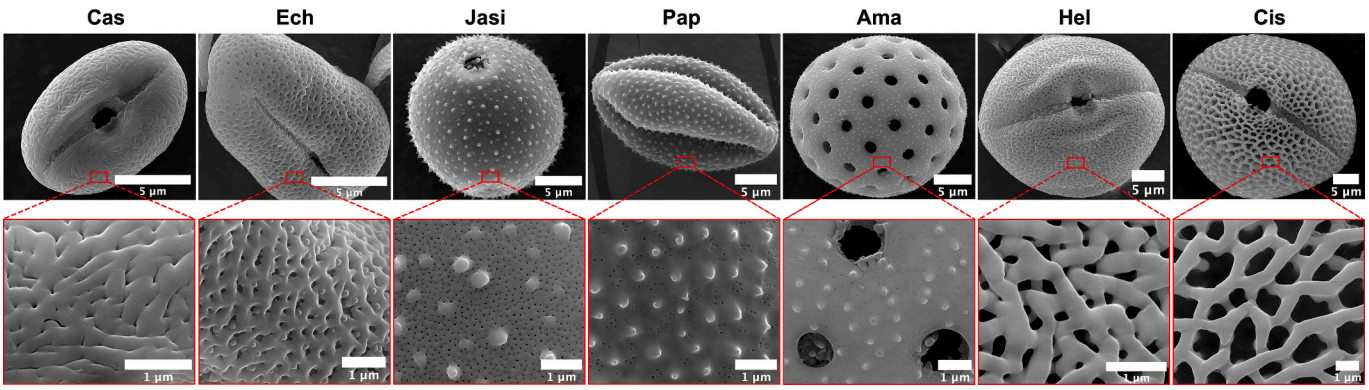

Fig. 9. SEM characterization of SMCs after exposure to in vitro simulated gastrointestinal tract and colonic fermentation conditions. The images confirm that SMCs maintain their structural integrity without significant degradation.

Table 2
Comparison between SMCs and microcapsules produced from other bio-derived polymers.

Loaded material	Microcapsule type	Size	Reported Results	Limitations relative to SMC	Ref
Resveratrol	Starch	228 µm	Drug loading capacity 11 %; sustained drug release at pH 1.2, and pH 7.0 reached 82 %	Non-uniform particle size and shape	[53]
Chlorpyrifos	Cellulose	3.8 µm	Loading efficiency of 33 wt%; thermal stimuli responsiveness, controlled release for up to 120 h	Low thermal stability and low 3D structural stability in a 45 % ethanol aqueous solution	[54]
Curcumin	Ethyl cellulose	107–158 µm	Microcapsules with 6–14 % loading capacity showed release performance up to 8 h, while drug release cumulative value reached 99 %	The produced microcapsules provide limited internal cavity	[55]
Vitamin E	Chitosan - sodium lauryl ether sulfate	5–7 µm	High encapsulation efficiency up to 100 % with crosslinking agents; rapid release profile of 80 % in the first 20 min	Non-uniform distribution associated with aggregate in some formulations; spray drying causes cracks, and requires cross-linking agents (e.g., glutaraldehyde, formaldehyde)	[56]
Bovine serum albumin	SMC (*Lycopodium clavatum*)	30 µm	43–59 % encapsulation efficiency with various loading techniques; rapid release at pH 1.2 and pH 7.4 without alginate coating; release of 90 % of the molecule in the first 5 min	–	[12]
Squalane and ovalbumin	SMC (Chrysanthemum)	28 µm	~75 % release of ovalbumin at pH 7.4 in 4 h	–	[17]
Aspirin	SMC (*Lycopodium clavatum*)	28 µm	53 % encapsulation efficiency; 52 % and 67 % release profile in 10 h at pH 1.2 and pH 7.4, respectively	–	[57]
Bovine serum albumin	SMC (*Pinus, Fraxinus excelsior* and *Tilia*)	30–39 µm, 18–22 µm, and 34–35 µm	Encapsulation efficiency ranging from 2 to 10 % with passive and centrifugal loading	–	[19]
5-FU	SMC (Cas, Ech, Jasi, Pap, Ama, Hel and Cis)	12–39 µm	Encapsulation efficiency ranging from 12 to 33 % with various loading techniques; rapid drug release ranging from 64 to 82 % in SGF in 2 h and following sustained drug release in SIF and SCF up to 24 h	–	*

* Present study.

Compared to previously studied *Lycopodium clavatum* based SMCs, which showed rapid release within the first five minutes [12], the SMCs in this study showed a more prolonged release, and >60 % of the drug was retained after one hour in simulated gastrointestinal conditions. These findings suggest that SMCs may serve as a viable alternative to conventional polymer-based drug carriers by offering a balance between encapsulation efficiency and controlled release.

The study reveals natural SMCs as promising carriers for drug delivery applications with potential advantages. The resistance of SMCs to digestive enzymes and colon bacteria further supports their stability in physiological environments, making them suitable for targeted drug delivery in the gastrointestinal tract. Future studies should investigate the optimization of SMCs functionalization to fine-tune release parameters for specific therapeutic applications.

3.4. Drug release kinetics of various SMCs

The drug release kinetics of the studied SMCs were analysed using zero-order, first-order, Higuchi, and Korsmeyer-Peppas models, Table 3. The best-fitting model for most formulations was the Korsmeyer-Peppas model, exhibiting the highest correlation coefficients (R^2 = 0.672–0.886). The release exponent (n) values ranged from 0.053 to 0.079, suggesting Fickian diffusion as the dominant release mechanism, consistent with previous studies on drug-loaded microcapsules [56,57]. The Higuchi model also showed relatively high R^2 values (0.657–0.849), supporting diffusion-controlled release behaviour. A previous study on *Lycopodium clavatum* SMCs loaded with aspirin reported a stronger correlation with these models, with Korsmeyer-Peppas kinetics governing the release (n = 0.176–0.443) and Higuchi model R^2 values ranging from 0.724 to 0.835, consistent with a Fickian diffusion transport mechanism in aspirin-loaded SMCs [57]. Similarly, *Corylus avellana* based SMCs have been shown to follow the Higuchi model with R^2 values above 0.839 rather than zero-order and first-order models, reinforcing that sporopollenin-based carriers primarily exhibit diffusion-dependent release [58].

The first-order model provided a better fit than zero-order kinetics,

Table 3
Kinetic parameters and model fit analysis of drug release for the SMCs under study.

SMC type	Zero-order kinetics		First-order kinetics		Higuchi model		Korsmeyer-Peppas model		
	R^2	k_0	R^2	k_1	R^2	k_H	R^2	k_{KP}	n
Cas	0.772	0.537	0.864	0.015	0.849	3.401	0.886	74.814	0.053
Ech	0.662	0.523	0.786	0.014	0.795	3.634	0.856	74.105	0.056
Jasi	0.695	0.514	0.806	0.012	0.796	3.324	0.866	73.109	0.054
Pap	0.631	0.554	0.710	0.011	0.657	3.420	0.672	67.281	0.058
Ama	0.606	0.732	0.845	0.024	0.711	4.791	0.785	72.948	0.079
Hel	0.757	0.567	0.810	0.010	0.759	3.432	0.731	64.377	0.058
Cis	0.749	0.526	0.811	0.008	0.821	3.327	0.861	60.968	0.063

R^2: correlation coefficient, k: release rate constant, n: release exponent.

indicated by higher R^2 values (0.710–0.864 vs. 0.606–0.772). Variations in release constants (k values) across formulations suggest that differences in microcapsule composition and structural properties influence drug diffusion rates. Notably, sample Ama type SMCs showed the highest k values, indicating a faster release profile, while Cis type SMCs exhibited the lowest values, suggesting prolonged drug retention. The lower correlation with the zero-order model in this study aligns with findings from sporopollenin-based carriers encapsulating pantoprazole and paracetamol, where release rates were not constant over time but were influenced by the porous nature of the microcapsules [58,59]. The variations observed across different SMC types suggest that morphological factors, such as size and aperture structure, significantly impact drug diffusion and release kinetics, corroborating findings from earlier studies on bio-derived microcapsules [55–57]. We cannot disregard that the initial burst release exceeding 50 % of the total drug is a handicap that strongly influences the kinetic model fitting, although the extent varies among SMC types. Nonetheless, this rapid release still reflects a modest diffusion barrier imparted by the SMC wall compared to the unencapsulated drug. To improve the drug-controlled release behaviour of these SMCs and guarantee a sustained profile within the target conditions, further optimization may be required, such as the application of polymer coatings to the SMCs surface, after drug loading, allowing.

4. Conclusions

We have demonstrated the feasibility of purifying natural SMCs with diverse sizes and species-specific uniform distribution from bee pollen pellets through a chemical method. This process offers a cost-effective and environmentally friendly means of creating microcarriers suitable for the loading and controlled release of orally administered drugs, such as 5-FU. The findings indicated that the vacuum loading technique yields the highest encapsulation efficiency compared to passive and compression techniques in general. The successful loading of 5-FU into SMCs was confirmed by FTIR spectroscopy and SEM analysis, revealing its presence within the internal cavities of the microcapsules. The morphology of the microcapsules influenced the encapsulation efficiency and the release profile of 5-FU in the gastrointestinal tract and colonic environments. Specifically, we observed that drug encapsulation efficiency increased with the size of SMCs, holding the number of pore-type apertures constant. Conversely, larger microcapsules exhibited a slower and more sustained release profile in simulated release environments. Variations in the number, size, and position of SMC apertures, such as in the case of Ama and Pap, resulted in differing encapsulation efficiencies and release rates. Our study also revealed that factors such as pH levels, digestive enzymes, and gut microbiota did not significantly affect the degradation of SMC microstructure.

These findings collectively offer insights into tailoring microcapsule types for specific release environments and rates based on their morphology. Furthermore, we highlight the potential for modifying SMCs with polymers to achieve finer control over drug release parameters. In conclusion, SMCs represent promising, practical, and versatile platforms for the targeted release of orally administered therapeutics in the gastrointestinal tract.

CRediT authorship contribution statement

Volkan Aylanc: Writing – review & editing, Writing – original draft, Visualization, Investigation, Conceptualization. **Andreia F. Peixoto:** Writing – review & editing, Methodology, Investigation. **Lalehan Akyuz:** Writing – review & editing, Validation, Methodology, Formal analysis. **Nuno Vale:** Writing – review & editing, Validation, Supervision. **Cristina Freire:** Writing – review & editing, Supervision, Resources. **Miguel Vilas-Boas:** Writing – review & editing, Supervision, Resources, Project administration, Funding acquisition, Conceptualization.

Declaration of competing interest

The authors declare that they have no known competing financial interests or personal relationships that could have appeared to influence the work reported in this paper.

Acknowledgements

The authors are grateful to the Foundation for Science and Technology (FCT, Portugal) for financial support by national funds FCT/MCTES to CIMO (UIDB/00690/2020 and UIDP/00690/2020), SusTEC (LA/P/0007/2021) and projects: UIDB/50006/2020, UIDB/04033/2020 and UIDP/50006/2020. Thanks to national funding, FCT for the CEEC contract (2020.01614.CEECIND/CP1596/CT0007) for Andreia F. Peixoto and the Ph.D. research grant for Volkan Aylanc (2021.07764.BD). Thanks to the NextGenerationEU recovery funds through the scope of Project BeeLand 10/C05-i03/2021.PPRR-C05-i03-I-000081.

Appendix A. Supplementary data

Supplementary data to this article can be found online at https://doi.org/10.1016/j.ijbiomac.2025.144384.

Data availability

Data will be made available on request.

References

[1] M.G. Bah, H.M. Bilal, J. Wang, Fabrication and application of complex microcapsules: a review, Soft Matter 16 (2020) 570–590, https://doi.org/10.1039/C9SM01634A.
[2] V. Aylanc, A.F. Peixoto, N. Vale, C. Freire, M. Vilas-Boas, Sporopollenin-based biomicrocapsules as green carriers for controlled delivery of pharmaceutical drugs, Appl. Mater. Today 33 (2023) 101860, https://doi.org/10.1016/j.apmt.2023.101860.
[3] D. Li, B. Liu, F. Yang, X. Wang, H. Shen, D. Wu, Preparation of uniform starch microcapsules by premix membrane emulsion for controlled release of avermectin, Carbohydr. Polym. 136 (2016) 341–349, https://doi.org/10.1016/j.carbpol.2015.09.050.
[4] A. Yunoki, E. Tsuchiya, Y. Fukui, A. Fujii, T. Maruyama, Preparation of inorganic/organic polymer hybrid microcapsules with high encapsulation efficiency by an

electrospray technique, ACS Appl. Mater. Interfaces 6 (2014) 11973–11979, https://doi.org/10.1021/am503030c.
[5] C.S. Pomelli, F. D'Andrea, A. Mezzetta, L. Guazzelli, Exploiting pollen and sporopollenin for the sustainable production of microstructures, New J. Chem. 44 (2020) 647–652, https://doi.org/10.1039/C9NJ05082E.
[6] P. Ghisellini, C. Cialani, S. Ulgiati, A review on circular economy: the expected transition to a balanced interplay of environmental and economic systems, J. Clean. Prod. 114 (2016) 11–32, https://doi.org/10.1016/j.jclepro.2015.09.007.
[7] M.G. Potroz, R.C. Mundargi, J.J. Gillissen, E.L. Tan, S. Meker, J.H. Park, H. Jung, S. Park, D. Cho, S.I. Bang, N.J. Cho, Plant-based hollow microcapsules for Oral delivery applications: toward optimized loading and controlled release, Adv. Funct. Mater. 27 (2017) 1700270, https://doi.org/10.1002/adfm.201700270.
[8] R.C. Mundargi, M.G. Potroz, S. Park, H. Shirahama, J.H. Lee, J. Seo, N.J. Cho, Natural sunflower pollen as a drug delivery vehicle, Small 12 (2016) 1167–1173, https://doi.org/10.1002/smll.201500860.
[9] D. Liu, T. Zhang, X. Cheng, B. Wang, Y. Guo, Z. Liu, H. Jiang, Y. Lu, D. Liu, B. Wang, Y. Guo, Z. Liu, Y. Lu, T. Zhang, H. Jiang, Engineering pollen-derived microstructures to reveal material Morpho-performance paradigm, Small 18 (2022) 2200037, https://doi.org/10.1002/smll.202200037.
[10] F.S. Li, P. Phyo, J. Jacobowitz, M. Hong, J.K. Weng, The molecular structure of plant sporopollenin, Nat Plants 5 (2018) 41–46, https://doi.org/10.1038/s41477-018-0330-7.
[11] T.F. Fan, S. Park, Q. Shi, X. Zhang, Q. Liu, Y. Song, H. Chin, M.S. Bin Ibrahim, N. Mokrzecka, Y. Yang, H. Li, J. Song, S. Suresh, N.J. Cho, Transformation of hard pollen into soft matter, Nat. Commun. 11 (2020) 1–10, https://doi.org/10.1038/s41467-020-15294-w.
[12] R.C. Mundargi, M.G. Potroz, S. Park, J.H. Park, H. Shirahama, J.H. Lee, J. Seo, N. J. Cho, Lycopodium spores: a naturally manufactured, Superrobust biomaterial for drug delivery, Adv. Funct. Mater. 26 (2016) 487–497, https://doi.org/10.1002/adfm.201502322.
[13] Y. Yang, W. Zhang, L. Zhang, M. Guo, C. Xiang, M. Ren, Y. Han, J. Shi, H. Li, X. Xu, The development of multifunctional materials for water pollution remediation using pollen and sporopollenin, Int. J. Biol. Macromol. 273 (2024) 133051, https://doi.org/10.1016/j.ijbiomac.2024.133051.
[14] A. De Mori, D. Quizon, H. Dalton, B. Yavuzyegit, G. Cerri, M. Antonijevic, M. Roldo, Sporopollenin capsules as biomimetic templates for the synthesis of hydroxyapatite and β-TCP, Biomimetics 9 (2024) 159, https://doi.org/10.3390/biomimetics9030159.
[15] N.M. Meligi, A.K.F. Dyab, Natural sporopollenin microcapsules: biological evaluation and application in regulating hepatic toxicity of diclofenac sodium in vivo, Biomater. Sci. 11 (2023) 6193–6209, https://doi.org/10.1039/D3BM00638G.
[16] M. Raish, M.A. Kalam, A. Ahmad, M. Shahid, M.A. Ansari, A. Ahad, R. Ali, Y.A. B. Jardan, A. Alshamsan, M. Alkholief, K.M. Alkharfy, I.A. Abdelrahman, F.I. Al-Jenoobi, Eudragit-coated sporopollenin exine microcapsules (SEMC) of *Phoenix dactylifera* L. of 5-fluorouracil for colon-specific drug delivery, Pharmaceutics 13 (11) (2021) 1921, https://doi.org/10.3390/pharmaceutics13111921.
[17] J. Liu, X.D. Yan, X.Q. Li, Y.H. Du, L.L. Zhu, T.T. Ye, Z.Y. Cao, Z.W. Dong, S.T. Li, X. Xu, W. Bai, D. Li, J.W. Zhang, S.J. Wang, S.H. Li, J. Sun, X.Z. Yin, Chrysanthemum sporopollenin: a novel vaccine delivery system for nasal mucosal immunity, Front. Immunol. 14 (2023) 1132129, https://doi.org/10.3389/fimmu.2023.1132129.
[18] A. Diego-Taboada, T. Sathyapalan, F. Courts, M. Lorch, F. Almutairi, B.P. Burke, K. Harris, M. Kruusmägi, T. Walther, J. Booth, A.N. Boa, S.J. Archibald, C. Thompson, S.L. Atkin, G. Mackenzie, Spore exines increase vitamin D clinical bioavailability by mucoadhesion and bile triggered release, J. Control. Release 350 (2022) 244–255, https://doi.org/10.1016/j.jconrel.2022.08.017.
[19] F.E. Atalay, A.A. Culum, H. Kaya, G. Gokturk, E. Yigit, Different plant Sporopollenin Exine capsules and their multifunctional usage, ACS Appl. Bio Mater. 5 (2022) 1348–1360, https://doi.org/10.1021/acsabm.2c00071.
[20] R. Liu, G.H. Ma, Y.H. Wan, Z.G. Su, Influence of process parameters on the size distribution of PLA microcapsules prepared by combining membrane emulsification technique and double emulsion-solvent evaporation method, Colloids Surf. B: Biointerfaces 45 (2005) 144–153, https://doi.org/10.1016/j.colsurfb.2005.08.004.
[21] D. Li, B. Liu, F. Yang, X. Wang, H. Shen, D. Wu, Preparation of uniform starch microcapsules by premix membrane emulsion for controlled release of avermectin, Carbohydr. Polym. 136 (2016) 341–349, https://doi.org/10.1016/j.carbpol.2015.09.050.
[22] T. Maric, M.Z.M. Nasir, N.F. Rosli, M. Budanović, R.D. Webster, N.J. Cho, M. Pumera, Microrobots derived from variety plant pollen grains for efficient environmental clean up and as an anti-Cancer drug carrier, Adv. Funct. Mater. 30 (2020) 2000112, https://doi.org/10.1002/adfm.202000112.
[23] M. Li, B. Hu, Z. Wu, Z. Wang, J. Weng, H. Zheng, L. Sun, Sporopollenin exine capsules modulate the function of microglial cells, Biomater. Sci. 12 (2024) 710–724, https://doi.org/10.1039/D3BM01154B.
[24] A.K. Prabhakar, M.G. Potroz, E.L. Tan, H. Jung, J.H. Park, N.J. Cho, Macromolecular microencapsulation using pine pollen: loading optimization and controlled release with natural materials, ACS Appl. Mater. Interfaces 10 (2018) 28428–28439, https://doi.org/10.1021/acsami.8b09952.
[25] S. Ertosun, V. Aylanc, A.F. Peixoto, A. Santamaria-Echart, P. Russo-Almeida, C. Freire, M. Vilas-Boas, Structural characterization of microcapsules from common bee pollen for the development of delivery systems, J. Polym. Environ. 33 (2024) 1171–1184, https://doi.org/10.1007/s10924-024-03478-0.
[26] V. Aylanc, S. Ertosun, A.F. Peixoto, A. Santamaria-Echart, P. Russo-Almeida, N. Vale, C. Freire, M. Vilas-Boas, Development of natural sporopollenin microcapsules: from bee pollen to versatile biomaterials, Emerg. Mater. (2025) 1–16, https://doi.org/10.1007/s42247-025-01002-1.
[27] R.C. Mundargi, E.L. Tan, J. Seo, N.J. Cho, Encapsulation and controlled release formulations of 5-fluorouracil from natural Lycopodium clavatum spores, J. Ind. Eng. Chem. 36 (2016) 102–108, https://doi.org/10.1016/j.jiec.2016.01.022.
[28] A.S. de Carvalho, S.C. de Rezende, C. Caleja, E. Pereira, L. Barros, I. Fernandes, Y. A. Manrique, O.H. Gonçalves, I.C.F.R. Ferreira, M.F. Barreiro, B-Carotene colouring systems based on solid lipid particles produced by hot melt dispersion, Food Control 129 (2021) 108262, https://doi.org/10.1016/j.foodcont.2021.108262.
[29] A. Brodkorb, L. Egger, M. Alminger, P. Alvito, R. Assunção, S. Ballance, T. Bohn, C. Bourlieu-Lacanal, R. Boutrou, F. Carrière, A. Clemente, M. Corredig, D. Dupont, C. Dufour, C. Edwards, M. Golding, S. Karakaya, B. Kirkhus, S. Le Feunteun, U. Lesmes, A. Macierzanka, A.R. Mackie, C. Martins, S. Marze, D.J. McClements, O. Ménard, M. Minekus, R. Portmann, C.N. Santos, I. Souchon, R.P. Singh, G. E. Vegarud, M.S.J. Wickham, W. Weitschies, I. Recio, INFOGEST static in vitro simulation of gastrointestinal food digestion, Nat. Protoc. 14 (2019) 991–1014, https://doi.org/10.1038/s41596-018-0119-1.
[30] Del J.N. Hierro, C. Cueva, A. Tamargo, E. Núñez-Gómez, M.V. Moreno-Arribas, G. Reglero, D. Martin, In vitro colonic fermentation of saponin-rich extracts from quinoa, lentil, and fenugreek. Effect on sapogenins yield and human gut microbiota, J. Agric. Food Chem. 68 (2020) 106–116, https://doi.org/10.1021/acs.jafc.9b05659.
[31] V. Aylanc, S. Ertosun, L. Akyuz, B. Koc Bilican, S. Gokdag, I. Bilican, Y.S. Cakmak, B.A. Yilmaz, M. Kaya, Natural β-chitin-protein complex film obtained from waste razor shells for transdermal capsaicin carrier, Int. J. Biol. Macromol. 155 (2020) 508–515, https://doi.org/10.1016/j.ijbiomac.2020.03.232.
[32] Mathematical models of drug release, in: M.L. Bruschi (Ed.), Strategies to Modify the Drug Release from Pharmaceutical Systems, Woodhead Publishing, 2015, pp. 63–86, https://doi.org/10.1016/B978-0-08-100092-2.00005-9.
[33] H. Lin, I. Gomez, J.C. Meredith, Pollenkitt wetting mechanism enables species-specific tunable pollen adhesion, Langmuir 29 (2013) 3012–3023, https://doi.org/10.1021/la305144z.
[34] P. Gonzalez-Cruz, M.J. Uddin, S.U. Atwe, N. Abidi, H.S. Gill, Chemical treatment method for obtaining clean and intact pollen shells of different species, ACS Biomater Sci. Eng. 4 (2018) 2319–2329, https://doi.org/10.1021/acsbiomaterials.8b00304.
[35] A. Lutzke, K.J. Morey, J.I. Medford, M.J. Kipper, Detailed characterization of Pinus ponderosa sporopollenin by infrared spectroscopy, Phytochemistry 170 (2020) 112195, https://doi.org/10.1016/j.phytochem.2019.112195.
[36] D. Li, L. Sun, L. Shi, L. Zhuo, L. Yang, J. Zhang, Y. Han, T. Ye, S. Wang, Reversible switchable wettability of intrinsic micro/nanostructured pollen microcarriers via pH-induce from superhydrophobicity to superhydrophilicity, Chem. Eng. J. 473 (2023) 145184, https://doi.org/10.1016/j.cej.2023.145184.
[37] D.L. Melnikova, Z.F. Badrieva, M.A. Kostin, C. Maller, M. Stas, A. Buczek, M. A. Broda, T. Kupka, A.M. Kelterer, P.M. Tolstoy, V.D. Skirda, On complex formation between 5-fluorouracil and β-Cyclodextrin in solution and in the solid state: IR markers and detection of short-lived complexes by diffusion NMR, Molecules 25 (2020) 5706, https://doi.org/10.3390/molecules25235706.
[38] M.J. Uddin, N. Abidi, J. Warzywoda, H.S. Gill, Investigation of the fate of proteins and hydrophilicity/hydrophobicity of Lycopodium clavatum spores after organic Solvent-Base-acid treatment, ACS Appl. Mater. Interfaces 11 (2019) 20628–20641, https://doi.org/10.1021/acsami.9b03040.
[39] L. Huang, W. Sui, Y. Wang, Q. Jiao, Preparation of chitosan/chondroitin sulfate complex microcapsules and application in controlled release of 5-fluorouracil, Carbohydr. Polym. 80 (2010) 168–173, https://doi.org/10.1016/j.carbpol.2009.11.007.
[40] M. Hadjianfar, D. Semnani, J. Varshosaz, Polycaprolactone/chitosan blend nanofibers loaded by 5-fluorouracil: an approach to anticancer drug delivery system, Polym. Adv. Technol. 29 (2018) 2972–2981, https://doi.org/10.1002/pat.4417.
[41] M. Yusefi, K. Shameli, H. Jahangirian, S.Y. Teow, H. Umakoshi, B. Saleh, R. Rafiee-Moghaddam, T.J. Webster, The potential anticancer activity of 5-fluorouracil loaded in cellulose fibers isolated from rice straw, Int. J. Nanomedicine 15 (2020) 5417–5432, https://doi.org/10.2147/IJN.S250047.
[42] M.J. Uddin, P. Gonzalez-Cruz, J. Warzywoda, H.S. Gill, Sporopollenin spikes augment antigen-specific immune response and generate long-lived humoral immunity, Adv. Ther. (Weinh.). 3 (2020) 2000102, https://doi.org/10.1002/adtp.202000102.
[43] A. Diego-Taboada, S.T. Beckett, S.L. Atkin, G. Mackenzie, Hollow Pollen Shells to Enhance Drug Delivery, Pharmaceutics 6 (2014) 80–96, 6 (2014) 80–96, https://doi.org/10.3390/pharmaceutics6010080.
[44] E.S. Hamilton, G.S. Jensen, G. Maksaev, A. Katims, A.M. Sherp, E.S. Haswell, Mechanosensitive channel MSL8 regulates osmotic forces during pollen hydration and germination, Science 350 (2015) (1979) 438–441, https://doi.org/10.1126/science.aac6014.
[45] R.D. Hoffmann, M.T. Portes, L.I. Olsen, D.S.C. Damineli, M. Hayashi, C.O. Nunes, J. T. Pedersen, P.T. Lima, C. Campos, J.A. Feijó, M. Palmgren, Plasma membrane H+-ATPases sustain pollen tube growth and fertilization, Nat. Commun. 11 (2020) 2395, https://doi.org/10.1038/s41467-020-16253-1.
[46] J.R. Rowley, J.J. Skvarla, G. El-Ghazaly, Transfer of material through the microspore exine - from the loculus into the cytoplasm, Can. J. Bot. 81 (2003) 1070–1082, https://doi.org/10.1139/b03-095.
[47] J.M. Lakkis, Encapsulation and controlled release applications in confectionery and oral care products, in: Encapsulation and controlled release technologies in food

systems: second edition, John Wiley & Sons, Ltd, 2016, pp. 236–288, https://doi.org/10.1002/9781118946893.ch9.
[48] C.E. Mora-Huertas, H. Fessi, A. Elaissari, Polymer-based nanocapsules for drug delivery, Int. J. Pharm. 385 (2010) 113–142, https://doi.org/10.1016/j.ijpharm.2009.10.018.
[49] H. Chen, C. Khemtong, X. Yang, X. Chang, J. Gao, Nanonization strategies for poorly water-soluble drugs, Drug Discov. Today 16 (2011) 354–360, https://doi.org/10.1016/j.drudis.2010.02.009.
[50] A. Solhjoo, Z. Sobhani, A. Sufali, Z. Rezaei, S. Khabnadideh, A. Sakhteman, Exploring pH dependent delivery of 5-fluorouracil from functionalized multi-walled carbon nanotubes, Colloids Surf. B: Biointerfaces 205 (2021) 111823, https://doi.org/10.1016/j.colsurfb.2021.111823.
[51] A. Merkli, J. Heller, C. Tabatabay, R. Gurny, The use of acidic and basic excipients in the release of 5-fluorouracil and mitomycin C from a semi-solid bioerodible poly (ortho ester), J. Control. Release 33 (1995) 415–421, https://doi.org/10.1016/0168-3659(94)00117-D.
[52] A.K.F. Dyab, M.A. Mohamed, N.M. Meligi, S.K. Mohamed, Encapsulation of erythromycin and bacitracin antibiotics into natural sporopollenin microcapsules: antibacterial, cytotoxicity, in vitro and in vivo release studies for enhanced bioavailability, RSC Adv. 8 (2018) 33432–33444, https://doi.org/10.1039/C8RA05499A.
[53] I. Choi, N. Li, Q. Zhong, Enhancing bioaccessibility of resveratrol by loading in natural porous starch microparticles, Int. J. Biol. Macromol. 194 (2022) 982–992, https://doi.org/10.1016/j.ijbiomac.2021.11.157.
[54] D. Xiao, W. Liang, Z. Xie, J. Cheng, Y. Du, J. Zhao, A temperature-responsive release cellulose-based microcapsule loaded with chlorpyrifos for sustainable pest control, J. Hazard. Mater. 403 (2021) 123654, https://doi.org/10.1016/j.jhazmat.2020.123654.
[55] X.C. Song, Y.L. Yu, G.Y. Yang, A.L. Jiang, Y. jie Ruan, S. hua Fan, One-step emulsification for controllable preparation of ethyl cellulose microcapsules and their sustained release performance, Colloids Surf. B: Biointerfaces 216 (2022) 112560, https://doi.org/10.1016/j.colsurfb.2022.112560.
[56] J.M. Budinčić, L. Petrović, L. Đekić, J. Fraj, S. Bučko, J. Katona, L. Spasojević, Study of vitamin E microencapsulation and controlled release from chitosan/sodium lauryl ether sulfate microcapsules, Carbohydr. Polym. 251 (2021) 116988, https://doi.org/10.1016/j.carbpol.2020.116988.
[57] A.S.Y. Mohammed, A.K.F. Dyab, F. Taha, A.I.A. Abd El-Mageed, Pollen-derived microcapsules for aspirin microencapsulation: in vitro release and physico-chemical studies, RSC Adv. 12 (2022) 22139–22149, https://doi.org/10.1039/D2RA02888C.
[58] L. Akyuz, I. Sargin, M. Kaya, T. Ceter, I. Akata, A new pollen-derived microcarrier for pantoprazole delivery, Mater. Sci. Eng. C 71 (2017) 937–942, https://doi.org/10.1016/j.msec.2016.11.009.
[59] M. Mujtaba, I. Sargin, L. Akyuz, T. Ceter, M. Kaya, Newly isolated sporopollenin microcages from Platanus orientalis pollens as a vehicle for controlled drug delivery, Mater. Sci. Eng. C 77 (2017) 263–270, https://doi.org/10.1016/j.msec.2017.02.176.